

Supplementary Material

Discreteness of Cell–Surface Contacts Affects Spatio-temporal Dynamics, Adhesion, and Proliferation of Mouse Embryonic Stem Cells

Esther Kimmle¹, Zahra Hajian Foroushani¹, Stephan Keppler², Judith Thoma¹, Kentaro Hayashi³, Akihisa Yamamoto³, Martin Bastmeyer^{2,3,4}, Motomu Tanaka^{1,3*}

¹Physical Chemistry of Biosystems, Institute of Physical Chemistry, Heidelberg University, 69120 Heidelberg, Germany

²Zoological Institute, Cell- and Neurobiology, Karlsruhe Institute of Technology, 76131 Karlsruhe, Germany

³Center for Integrative Medicine and Physics, Institute for Advanced Study, Kyoto University, 6068501 Kyoto, Japan

⁴Institute for Biological and Chemical Systems - Biological Information Processing (IBCS-BIP), Karlsruhe Institute of Technology, 76344 Eggenstein-Leopoldshafen, Germany

*** Correspondence:**

Motomu Tanaka

tanaka@uni-heidelberg.de

1 Supplementary Data

Supplementary Data S1. Specific and non-specific adhesion of mESCs.

To check the specific and non-specific adhesion of mESCs on bare glass, we incubated mESCs on bare glass substrates with no pre-treatment for 4 h and compared the amount of cells on the surface with that on gelatin-coated glass substrates. As presented in Figure S1, the density of cells on the surface was much less on bare glass than those on gelatin-coated glass. It is notable that the cells non-specifically adhered on bare glass formed aggregates, suggesting that non-specific cell-glass interactions are weaker than cell-cell interactions.

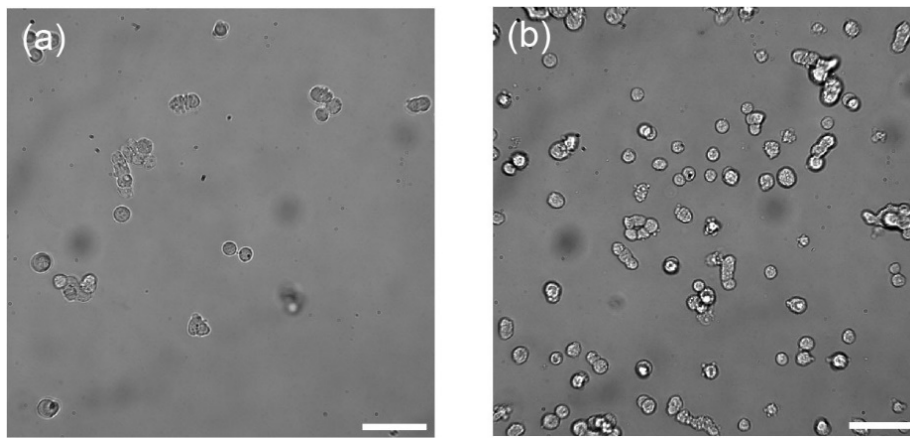


Figure S1 Brightfield images of Oct4-GFP mESCs on a bare glass substrate (a) and a glass substrate continuously coated with gelatin (b). Scale bars: 50 μm .

Supplementary Data S2. Timelapse movies of Oct4-GFP mESCs on three different surfaces

Movie S2 Timelapse movies for 150 min of Oct4-GFP mESCs on (a) dense and (b) sparse GNFs as well as on continuous gelatin (c).

Supplementary Data S3. Scanning electron micrographs of dry GNFs

The structures of dry GNFs before and after the chemical crosslinking in EtOH solution were characterized using a Zeiss Leo 1530 scanning electron microscope (Zeiss, Oberkochen, Germany).

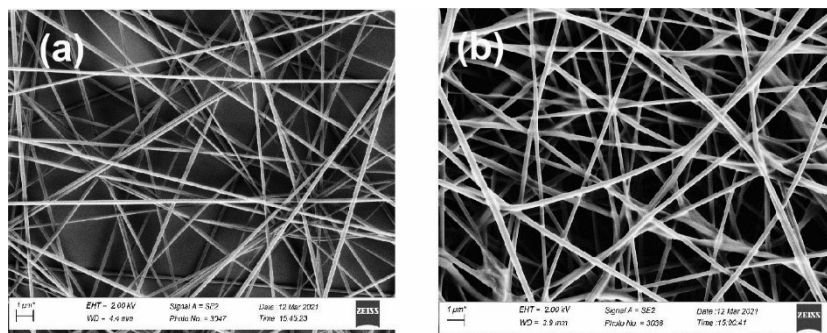


Figure S3. Scanning electron micrographs of GNFs (a) before and (b) after the chemical crosslinking in EtOH. Scale bars: 1 μm .

Supplementary Data S4. Force map of GNFs measured by a pyramidal cantilever.

The force map of GNFs was measured by a pyramidal tip used for the topographic profile analysis. The distribution of the measured Young's moduli fitted with a Lorentzian function (blue line), yielding $\langle E \rangle = 489$ kPa. It should be noted that the use of a pyramidal tip resulted in an overestimation of the Young's modulus with a broader distribution.

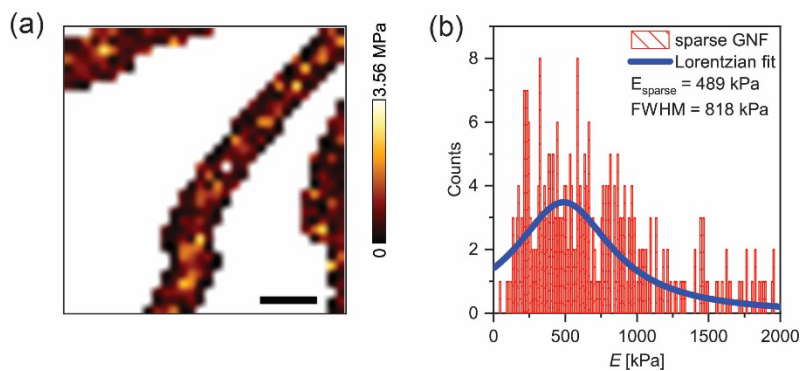


Figure S4. (a) Force map and (b) distribution of GNFs measured with a pyramidal cantilever. Scale bar: 1 μm . Compared to the data obtained with a particle-assisted cantilever (Figure 1), the use of a pyramidal tip resulted in an overestimation of Young's modulus with a broader distribution.

Supplementary Data S5. Fluorescence image of the glass surface continuously coated with gelatin

To confirm the uniform, continuous functionalization with gelatin, a glass-bottomed petri dish was incubated with a 2 mL portion of FITC-gelatin (Eurogentec, Köln, Germany) dissolved in PBS (0.1 wt%) for 30 min, following the same protocol as we used throughout this study. The unbound gelatin was washed off with 2 mL PBS.

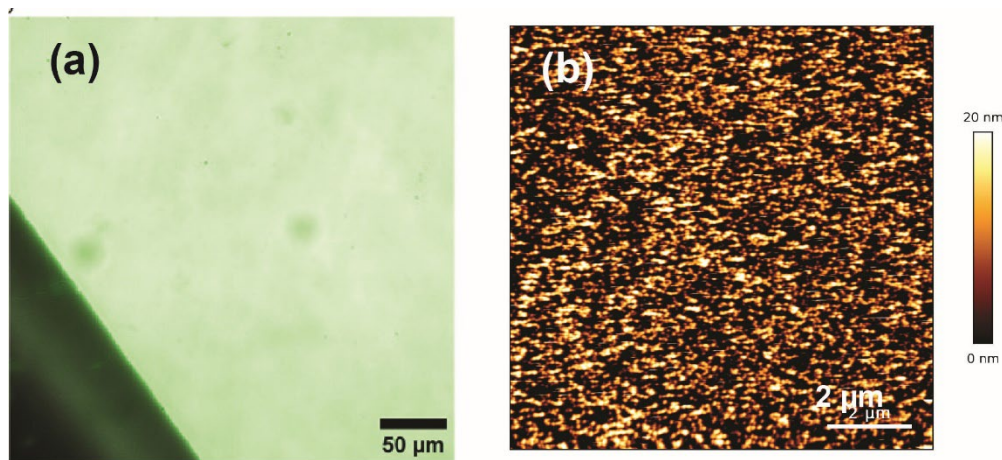


Figure S5. (a) Fluorescence image and (b) AFM topographic profile of the glass surface coated with FITC-conjugated gelatin. The region near the edge of the glass surface was visualized to highlight the difference from the background (black). The topographic profile of the gelatin layer was characterized by contact mode AFM with a pyramidal tip ($k = 0.03$ N/m). Scale bars: 50 μm (a), 2 μm (b). RMS roughness value of gelatin-coated surface was 5.7 ± 1.4 nm.

Supplementary Data S6. Comparison of cell phenotypes with and without fluorescence illumination.

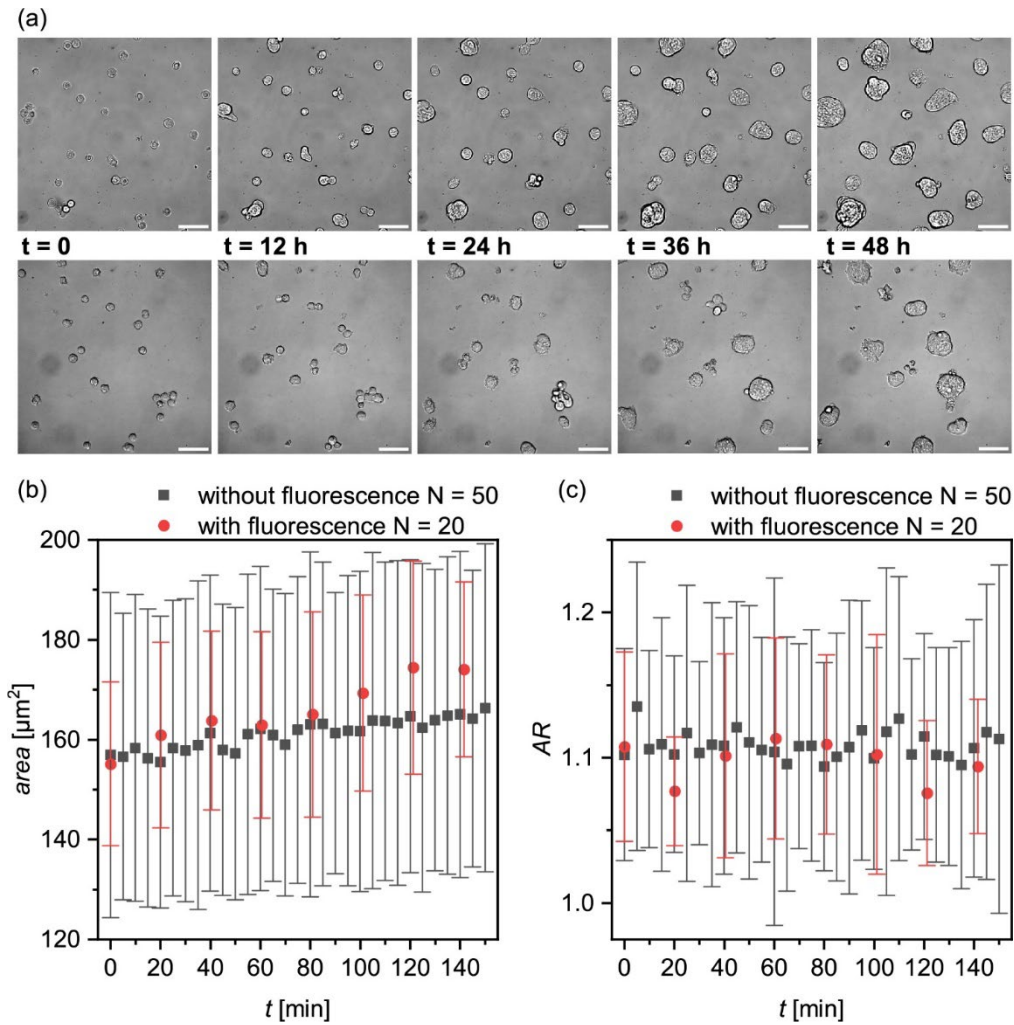


Figure S6 (a) Snapshot images of Oct4-GFP mESCs on continuous gelatin of timelapse with (upper row) and without (lower row) fluorescence, scale bars: 50 μm . Area (b) and AR (c) of timelapse images on continuous gelatin with and without fluorescence analysed by hand. Mean values of both are not significantly different.

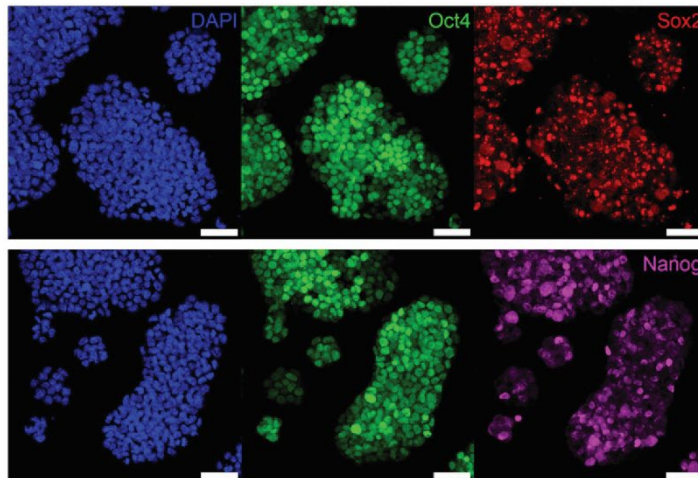
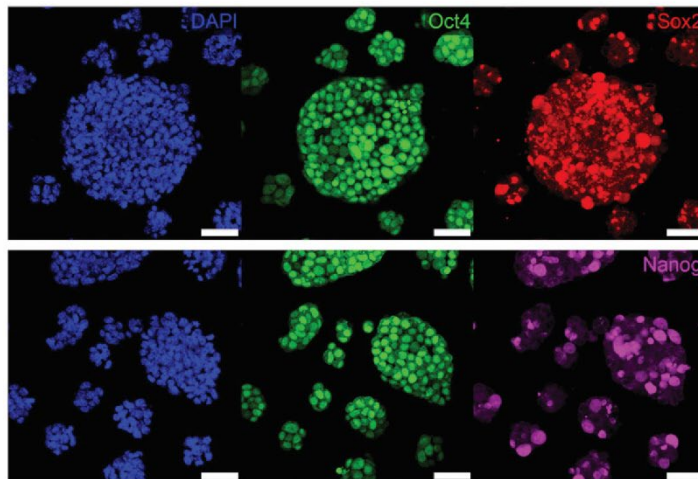
Supplementary Data S7. Maintenance of pluripotency on the other surfaces.**(a) Dense GNF****(b) Continuous gelatin**

Figure S7. Fluorescence images of Oct4-GFP mESCs at $t = 48$ h on (a) dense GNFs and (b) continuous gelatin, blue: DAPI, green: Oct4-GFP reporter, red: anti-Sox2, magenta: anti-Nanog. Scale bars: 50 μm .

Supplementary Data S8. Analyses of mean square displacement of mESCs.

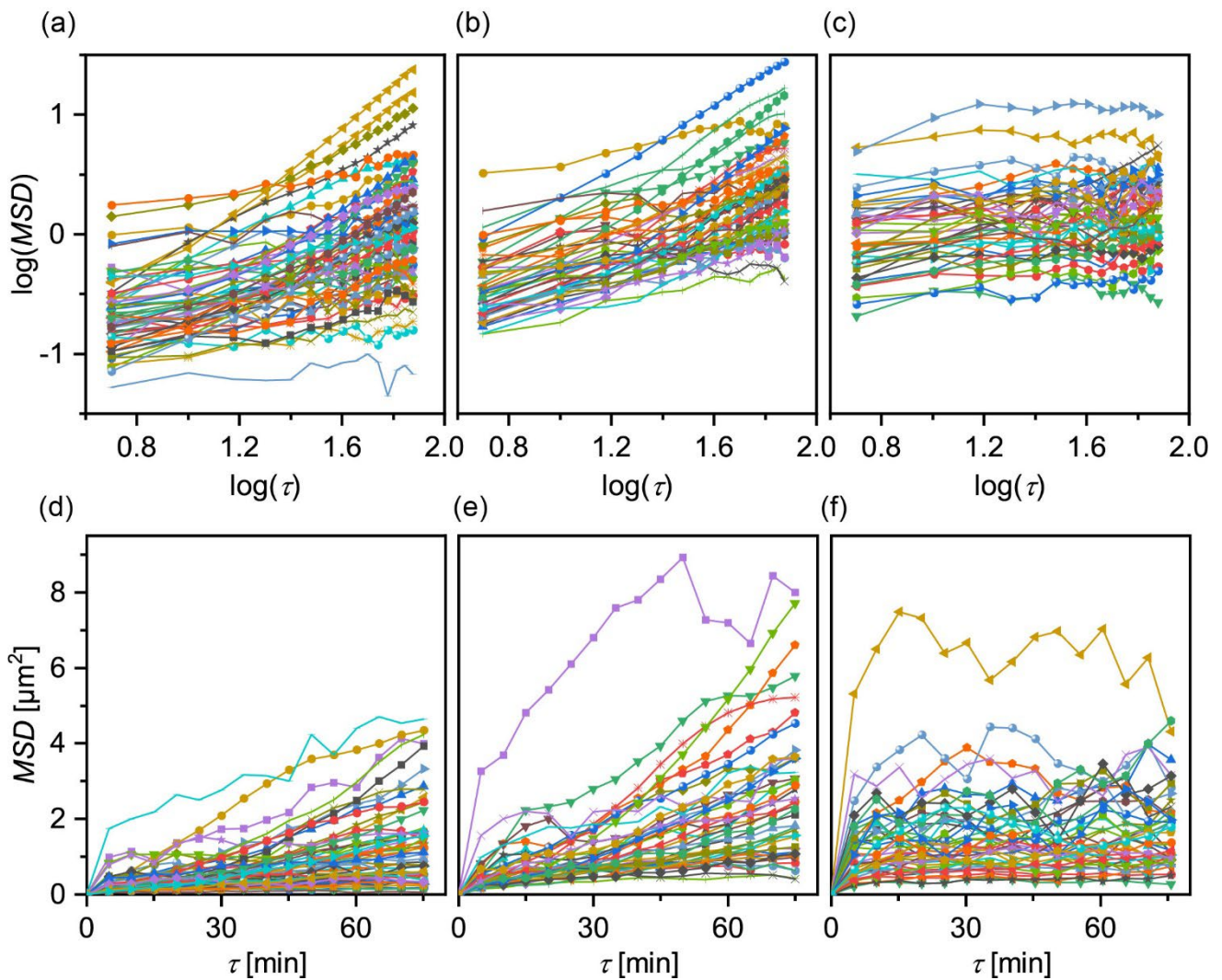


Figure S8. Mean squared displacements (MSD) of Oct4-GFP mESCs on (a) dense and (b) sparse GNFs as well as on continuous gelatin (c) double logarithmic plots, yielding the power law exponent α . The same data plotted in linear plot (d - f) were used to calculate the diffusion coefficient D .

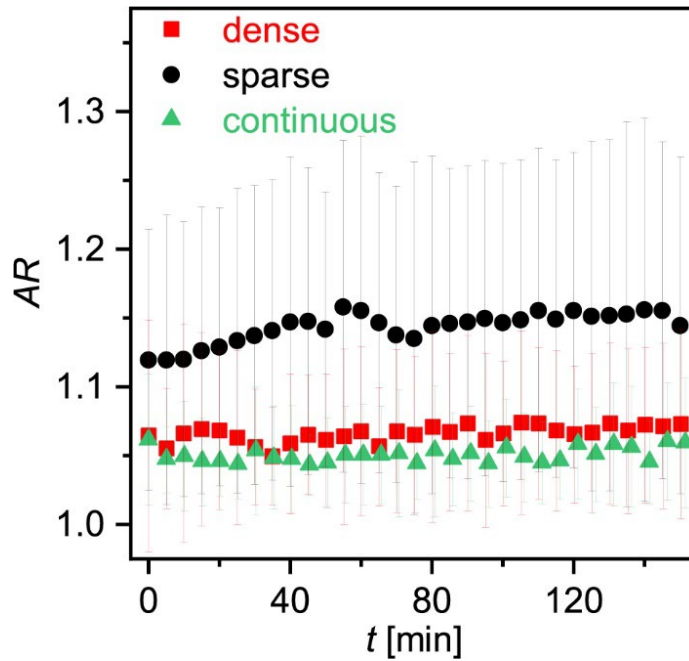
Supplementary Data S9. Morphometric parameter (aspect ratio, AR) recorded over time.

Figure S9. Aspect ratio (AR) of Oct4-GFP mESCs on three surfaces plotted versus time. The values on sparse GNFs were always larger than those on the other two surfaces, which is in good agreement with the data presented in Figure 5.

Supplementary Data S10. Calibration of pressure P versus the pulse energy E and the distance from the focal point d .

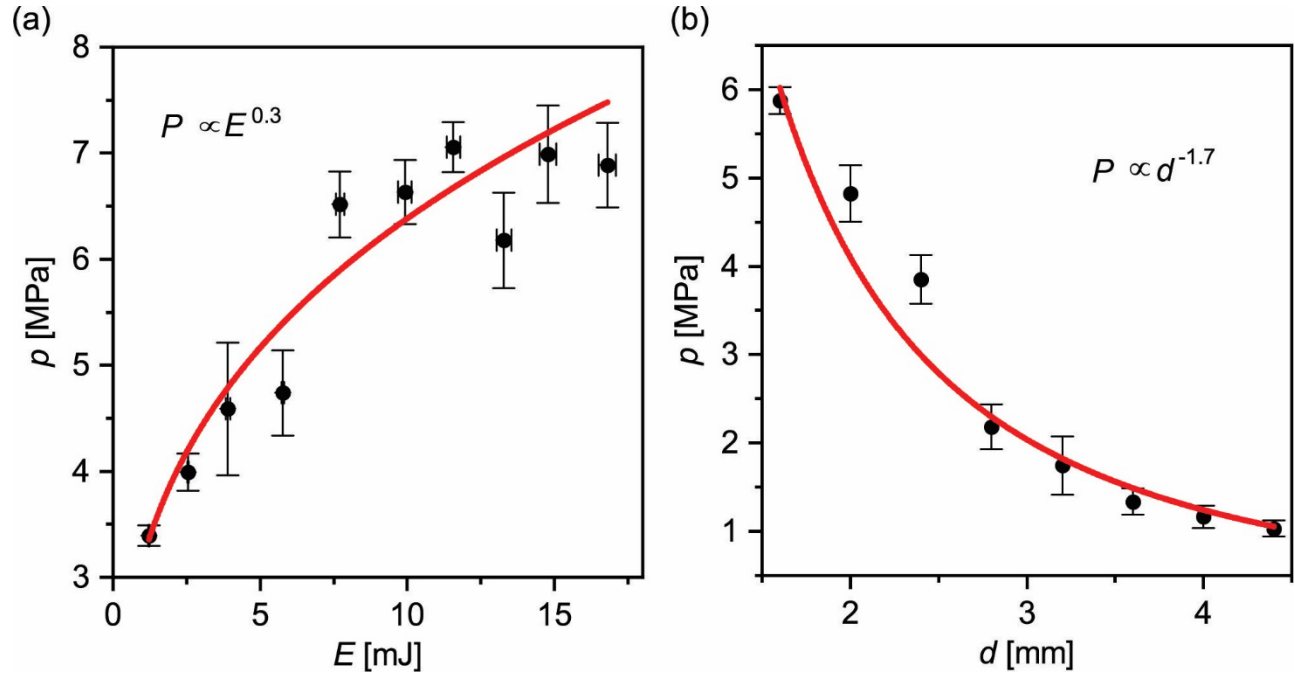


Figure S10. (a) Plot of pressure P monitored by a pressure sensor plotted versus the laser pulse energy E . Here the detector was placed at a distance of $d = 1.6$ mm from the focal point. (b) P plotted versus the distance from the focal point d , by setting the pulse energy constant at $E = 16.4$ mJ.